Eur Biophys J (2002) 31: 504–520
DOI 10.1007/s00249-002-0243-1

ARTICLE

Iris Antes · Walter Thiel · Wilfred F. van Gunsteren

Molecular dynamics simulations of photoactive yellow protein (PYP) in three states of its photocycle: a comparison with X-ray and NMR data and analysis of the effects of Glu46 deprotonation and mutation

Received: 28 September 2001 / Revised: 6 June 2002 / Accepted: 6 June 2002 / Published online: 18 October 2002

Abstract Photoactive yellow protein (PYP) is a prototype of the PAS domain superfamily of signaling proteins. The signaling process is coupled to a three-state photocycle. After the photoinduced *trans-cis* isomerization of the chromophore, 4-hydroxycinnamic acid (pCA), an early intermediate (pR) is formed, which proceeds to a second intermediate state (pB) on a sub-millisecond time scale. The signaling process is thought to be connected to the conformational changes upon the formation of pB and its recovery to the ground state (pG), but the exact signaling mechanism is not known. Experimental studies of PYP by solution NMR and X-ray crystallography suggest a very flexible protein backbone in the ground as well as in the signaling state. The relaxation from the pR to the pB state is accompanied by the protonation of the chromophore's phenoxyl group. This was found to be of crucial importance for the relaxation process. With the goal of gaining a better understanding of these experimental observations on an atomistic level, we performed five MD simulations on the three different states of PYP: a 1 ns simulation of PYP in its ground state [pG(MD)], a 1 ns simulation of the pR state [pR(MD)], a 2 ns simulation of the pR state with the chromophore protonated (pRprot), a 2 ns simulation of the pR state with Glu46 exchanged by Gln (pRGln) and a 2 ns simulation of PYP in its signaling state [pB(MD)]. Comparison of the pG simulation results with X-ray and NMR data, and with the results obtained for the pB simulation, confirmed the experimental observations of a rather flexible protein backbone and conformational changes during the recovery of the pG from the pB state. The conformational changes in the region around the chromophore pocket in the pR state were found to be crucially dependent on the strength of the Glu46-pCA hydrogen bond, which restricts the mobility of the chromophore in its unprotonated form considerably. Both the mutation of Glu46 with Gln and the protonation of the chromophore weaken this hydrogen bond, leading to an increased mobility of pCA and large structural changes in its surroundings. These changes, however, differ considerably during the pRGln and pRprot simulations, providing an atomistic explanation for the enhancement of the rate constant in the Gln46 mutant.
Electronic Supplementary Material is available if you access this article at http://dx.doi.org/10.1007/s00249-002-0243-1. On that page (frame on the left side), a link takes you directly to the supplementary material.

Keywords Photoactive yellow protein · Molecular dynamics · Photocycle · Protonation

Electronic Supplementary Material is available if you access this article at http://dx.doi.org/10.1007/s00249-002-0243-1. On that page (frame on the left side), a link takes you directly to the supplementary material.

I. Antes · W.F. van Gunsteren (✉)
Laboratory of Physical Chemistry,
Swiss Federal Institute of Technology Zürich,
ETH-Zentrum, 8092 Zurich, Switzerland
E-mail: wfvgn@igc.phys.chem.ethz.ch

I. Antes · W. Thiel
Institute of Organic Chemistry, University of Zürich,
Winterthurer Strasse 190, 8057 Zurich, Switzerland

Present address: I. Antes
Department of Chemistry, University of California,
Berkeley, CA 94720, USA

Present address: W. Thiel
Max-Plank-Institut für Kohlenforschung,
Kaiser-Wilhelm-Platz 1, 45470 Mulheim an der Ruhr, Germany

Introduction

Photoactive yellow protein (PYP) is a small (125-residue) light-sensitive protein which is thought to be involved in the negative phototaxis of the bacterium *Ectothiorhodospira halophila* (Sprenger et al. 1993). Its chromophore, 4-hydroxycinnamic or *p*-coumaric acid (pCA), is bound through a thioester linkage to Cys69 of

PYP (Baca et al. 1994; Hoff et al. 1994a). In the ground state, pG, the protein has an absorbance maximum at $\lambda_{max} = 446$ nm (Meyer 1985), giving it a yellow color. Upon excitation by light, the chromophore conformation around the C7-C8 double bond switches from *trans* to *cis* (Kort et al. 1996), causing the protein to adopt within nanoseconds a red-shifted transient state pR with $\lambda_{max} = 465$ nm (Meyer et al. 1987, 1989; Van Beeumen et al. 1993; Hoff et al. 1994b; Imamoto et al. 1996). This process proceeds through two short-lived intermediates I_0 and $I_0^{\ddagger}$ (Ujj et al. 1998). The pR state then converts on a submillisecond time scale into a blue-shifted or bleached transient state, pB, with $\lambda_{max} = 355$ nm. During this step the chromophore is protonated and the residue Glu46, which forms a hydrogen bond with the unprotonated chromophore in pR, is deprotonated. pB subsequently relaxes back to the pG state on a subsecond time scale (Meyer et al. 1987, 1989; Hoff et al. 1994b). This photocycle is summarized in Fig. 1. The phototropic signal transduction pathway is not known, but the change in PYP conformation occurring upon the formation of the pB state and its relaxation back to the ground state pG are thought to be responsible for relaying the signal to the next shackle in the signal transduction chain, which is assumed to involve protein-protein interaction with an as-yet unknown protein (Hoff et al. 1999). Sequence alignment studies have identified PYP as a prototype for the PAS domain superfamily of signaling proteins (Pellequer et al. 1998). Since PYP is a relatively small water-soluble protein, it is very suitable to study the molecular mechanism of signal transduction through an analysis of the structural and dynamical features of the states of the photocycle.

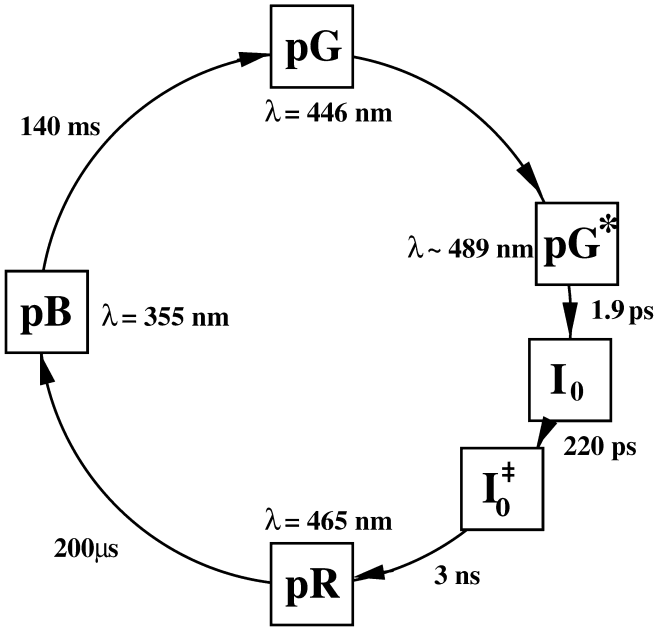

Fig. 1 Photocycle of PYP in solution. *pG*: ground state; *pR*: red-shifted state; *pB*: blue-shifted signaling transient state. The *numbers* indicate the wavelength of maximum absorption in nm (Hoff et al. 1994b)

The ground state structure of PYP has been determined by X-ray crystallography (Borgstahl et al. 1995; Genick et al. 1998; van Aalten et al. 2000) and by solution NMR (Düx et al. 1998) (see Fig. 2). X-ray crystallographic structures are also available for the PYP_{BL} and pB states (Genick et al. 1997a, 1998) and for the pR state (Perman et al. 1998); the latter, however, was recently reassigned to an earlier intermediate (Ren et al. 2001). In addition, a series of time-resolved X-ray Laue diffraction structures were measured for the time from 1 ns up to seconds after the photoexcitation (Ren et al. 2001). The latter study suggests that the spectroscopic pR state consists of several closely related conformers, which are structurally very similar to the PYP_{BL} state. The PYP_{BL} state is a low-temperature (< 90 K) state which does not exist at room temperature; its absorption at 400 nm, however, and its very strong structural similarity to the pR state conformers, suggest that it corresponds to an early conformer of the pR state at room temperature. Several other experimental studies have provided additional information on the variation of protein conformation and protonation states along the photocycle (Xie et al. 1996, 2001; Genick et al. 1997b; Imamoto et al. 1997; Hoff et al. 1999; Hendriks et al. 2002). In this work we are mainly referring to three experimental observations. First, there are significant local structural differences between the crystal structure (Borgstahl et al. 1995) of the ground state of PYP determined using X-ray diffraction and the ensemble of solution structures (Düx et al. 1998) determined using NMR spectroscopy, especially around the chromophore pocket and the N-terminal cap of the protein. Second, an NMR study of the pB state revealed considerable disorder (Rubinstenn et al. 1998), in contrast to the X-ray crystallographic data (Genick et al. 1997a; Ren et al. 2001). Third, the mechanism of the protonation of the chromophore after the photoexcitation is not resolved yet. There has been increasing evidence for the important role of the Glu46 residue. This residue forms a hydrogen bond with the phenoxyl oxygen (O1) of the unprotonated chromophore (Fig. 2) in the pG and pR states and a proton transfer from Glu46 to the chromophore has been proposed during the pR-pB transition (Xie et al. 1996, 2001; Imamoto et al. 1997; Hendriks et al. 1999). In addition, mutation experiments have shown changes in the magnitude and pH dependence of the rate constants of the process, if Glu46 is exchanged for Gln46. Information on pK_a values can be obtained from a combination of measurements (Xie et al. 1996; Genick et al. 1997b ; Imamoto et al. 1997). Computational studies may yield a picture of conformational and dynamical changes along the photocycle at the atomic level and thereby contribute to the resolution of these issues.

Photoexcitation of the chromophore in a simple model environment has been studied using quantum-chemical methodology (He et al. 2000). Structural relaxation of the chromophore environment on a picosecond time scale after photoexcitation has been studied using molecular dynamics (MD) simulations (Yamato

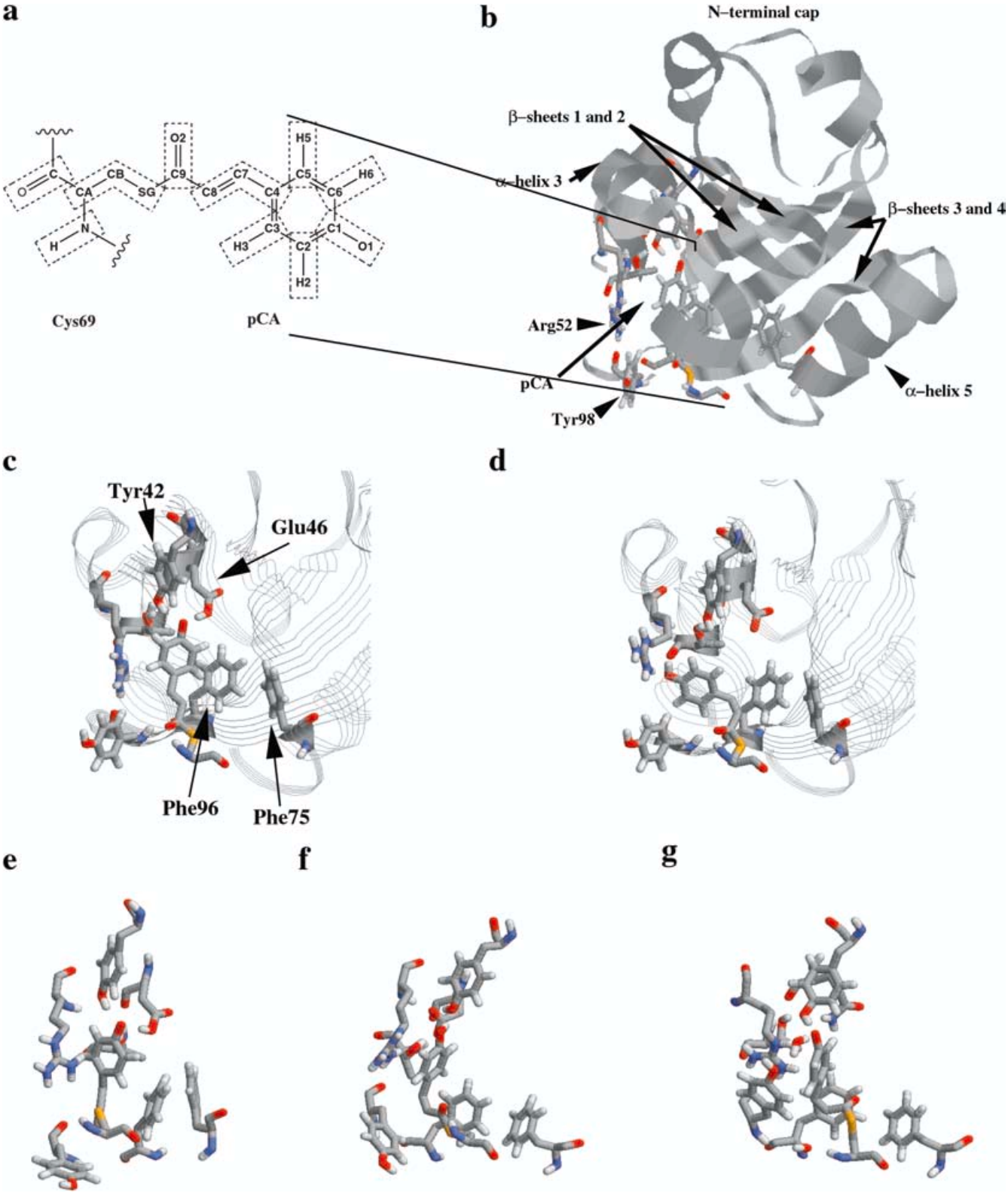

et al. 1998). MD simulations of PYP in aqueous solution in its ground state and the chromophore in *cis* conformation over 400 ps have been analyzed using normal mode analysis or so-called essential dynamics in order to identify global conformational changes which might be identical with the conformational changes occurring along the photocycle (van Aalten et al. 1998). The same normal mode analysis technique has been applied to sets of NMR and X-ray structures in order to characterize their conformational variation (van Aalten et al. 2000).

Fig. 2 (**a**) Structure diagram and atom names of Cys69 and the *p*-coumaric acid (pCA) chromophore linked to it. The *dashed lines* indicate so-called charge groups of the GROMOS96 force field (van Gunsteren et al. 1996). (**b**) Ribbon diagram of the three-dimensional structure of the ground state of PYP as determined by X-ray crystallography (Borgstahl et al. 1995). The chromophore (pCA) bound to Cys69 and the key active site residues Tyr42, Glu46, Thr50, Arg52, Phe75, Phe 96 and Tyr98 are shown in atomic detail. (**c–g**) Schematic diagrams of positions of the key residues around the chromophore pocket for the pG(X-ray) (**c**) and pB(X-ray) (**d**) structures and for the final structures of the pR(MD) (**e**), pRp(MD) (**f**) and pRGln(MD) (**g**) simulations. For nomenclature, see legend to Table 1

Functionally important protonation states of PYP, the interactions that stabilize them, and changes in the protonation state during the photocycle have been studied using continuum electrostatic theory (Demchuk et al. 2000). Finally, the structural fluctuations in the pB state were studied using molecular dynamics techniques (Shiozawa et al. 2001).

Here, an extensive MD simulation study of PYP in its three states of the photocycle is reported, allowing us a direct comparison of the structural differences/changes in the three states. First, the structures from a 1 ns MD trajectory of the ground state (pG) are compared to X-ray crystal and NMR solution data. In the pG simulation the chromophore (pCA) is deprotonated and Glu46 is protonated. Second, MD simulations of the ground state (pG) and of the blue-shifted signaling state (pB) are compared with each other to detect structural and dynamical differences. In the pG simulation the chromophore (pCA) is deprotonated and Glu46 is protonated, whereas in the pB simulation Glu46 is deprotonated and pCA protonated. Third, the importance of the protonation state of the chromophore and the Glu46 residue hydrogen-bonded to it is studied by comparison of the pR simulation, in which the chromophore (pCA) is deprotonated and Glu46 is protonated with a simulation (pRprot), in which the chromophore (pCA) is protonated and Glu46 deprotonated. Finally, the effect of the mutation of Glu46 into Gln46 is studied by a comparison of the pR simulation with a simulation (pRGln) in which Glu46 is replaced by Gln46. For the simulations of he protonated structure (pRprot) and the mutant (pRGln) the 3PYP crystal structure is used, with the chromophore protonated and Glu46 exchanged by Gln46, respectively. The five MD simulations yield an insight into structural relaxation of the various states along the photocycle and into the effects of (de)protonation and mutation of Glu46.

Materials and methods

The simulations and the analysis of the five PYP trajectories were carried out using the GROMOS96 program package (van Gunsteren et al. 1996; Scott et al. 1999). The protein was modeled using the GROMOS96 force field version 43A1. In this force field, aliphatic CH groups are modeled as united atoms. The force field parameters of the chromophore were chosen in a way analogous to that for the protein residues (Supplementary material, Table S1). The water molecules were modeled using the simple point charge (SPC) model (Berendsen et al. 1981) for liquid water. Three different sets of initial protein structures were used (Supplementary material, Table S2): these were the crystal structure of the ground state (Borgstahl et al. 1995) for the pG simulation, that of the low-temperature red-shifted state PYP_{BL} (Genick et al. 1998) for the pR simulations, and that of the blue-shifted state (Genick et al. 1997a) for the pB simulation. The PYP_{BL} structure was used for the pR simulations, because its structure agrees very well with the pR conformers at room temperature (see Introduction). In all simulations, truncated octahedral periodic boundary conditions were used. The computational boxes contained 1268 or 1269 protein atoms, 7 sodium ions and 4838, 5114 or 4834 water molecules, respectively. The initial length of the box edges was 6.89 nm.

To allow the relaxation of the water around the protein, a temperature of 100 K was used for the first 5 ps and 200 K for the next 5 ps; the simulation was then continued at 298.15 K. The positions of the protein atoms were restrained for the first 100 ps of the run. After that the simulations were continued without any position restraints and with a constant pressure of 1 atm throughout. The temperature and pressure were maintained by weak coupling to an external bath with a temperature coupling relaxation time of 0.1 ps and a pressure coupling relaxation time of 0.5 ps (Berendsen et al. 1984). An isothermal compressibility of 45.75×10^{-5} (kJ mol^{-1} nm^{-3})$^{-1}$ was used. Throughout the simulations the bond lengths were constrained to ideal values using the SHAKE procedure (Ryckaert et al. 1977), with a geometric accuracy of 10^{-4}. For the non-bonded interactions, a triple-range method with cutoff radii of 0.8 nm and 1.4 nm was used (Scott et al. 1999). Within the short-range cutoff of 0.8 nm, all interactions were determined every step. Longer range (electrostatic and van der Waals) interactions within a cutoff range of 1.4 nm were updated at the same time as the pair list for short-range interactions was updated (every 10 fs). A reaction field approximation (Tironi et al. 1995) was applied beyond a cutoff of 1.4 nm with a relative dielectric permittivity of 54.0 for SPC water (Smith and van Gunsteren 1994). A time step of 2 fs was used. The analysis was performed using the trajectory coordinates and energies that were written to disk every 0.1 ps for the 500–1000 ps simulation period for pG and pR and for the 500–2000 ps simulation period for pRprot, pRGln and pB.

Results

First, we will compare our simulation [pG(MD)] results for the ground state structure pG with the corresponding X-ray [pG(X-ray)] and NMR [P(NMR)] structure. This is of special interest because the local structural differences between the experimental data are rather pronounced (Düx et al. 1998; van Aalten et al. 2000), indicating a high backbone flexibility. In addition, this will allow us to judge the overall performance of our simulations. In the second part, we will examine the changes in the secondary structure of the protein related to the structural changes around the chromophore by comparing our simulations of the ground state pG(MD) with our results for the signaling state pB(MD). Lastly, we will study the dynamics of the chromophore after excitation [pR(MD)], its dependence on the protonation state [pRprot(MD)], and the influence of Glu46 [pRGln(MD)].

Comparison of the ground state structures

Comparison of the experimental structures

Previous studies have shown significant local structural differences between the experimentally obtained structures of PYP in its ground, as well as in its signaling state (Düx et al. 1998; Rubinstenn et al. 1998; van Aalten et al. 1998, 2000). These differences are especially pronounced around the chromophore pocket and the N-terminus of the protein (Borgstahl et al. 1995; Düx et al. 1998; Genick et al. 1998; Rubinstenn et al. 1998). Also the X-ray structures can differ considerably from each other in these protein regions, depending on the space group of crystallization (van Aalten et al. 2000), although the overall r.m.s. atom-positional deviation between these measured structures is still 0.048 nm. Here we compare the X-ray crystal structure of the ground state of PYP, which we used as starting structure for our solution simulation (Borgstahl et al. 1995) and the NMR solution structures measured by Düx et al. (1998). In Table 1 we give the overall r.m.s. atom-positional deviation between the X-ray, the NMR and the average simulated structures. Between the experimental structures the overall differences are up to 0.314 nm for the C_α atoms and up to 0.373 nm for all atoms, respectively. These differences are shown in more detail in Fig. 3 (panels a and b). In these panels the r.m.s. atom-positional deviations between the X-ray and the NMR structures are given for the outermost side-chain atoms and the C_α atoms of the individual residues. The largest deviations are found at the N-terminal region of the protein's backbone, which strongly contributes to the overall deviations of over 0.3 nm (see Table 1). For the remainder of the protein the deviations for the C_α atoms are 0.12 nm. This is in agreement with the reported r.m.s. atom-positional deviation of 0.188 nm for all heavy atoms between the NMR and crystal structure if the N-terminus is excluded (Düx et al. 1998).

Table 1 Atom-positional root-mean-square differences (r.m.s.d.) between various pairs of structures. The structures are superimposed using a translational/rotational fit involving all C_α atoms. Part (a): r.m.s.d. values for C_α atoms. Part (b): r.m.s.d. values for all atoms. pG(X-ray): crystal structure of the ground state (PDB code 2PHY); pB(X-ray): crystal structure of the blue-shifted or signaling state (PDB code 2PYP); pG(NMR): solution structure of the ground state (PDB code 3P HY); pG(MD): average structure obtained from the 500–1000 ps period of the pG simulation; pB(MD): average structure obtained from the 500–2000 ps period of the pB simulation; PYP_{BL}(X-ray): crystal structure of the red shifted (or I_1) state (PDB code 3PYP); pR(MD): average structure obtained from the 500–1000 ps period of the pR simulation; pRprot(MD): average structure obtained from the 500–2000 ps period of the pRprot simulation; pRGln(MD): average structure obtained from the 500–2000 ps period of the pRGln simulation

(a)		**X-ray pG**	**X-ray pB**	**NMR pG**	**MD pG**	**MD pB**
X-ray	pG	0.000	0.011	0.314[a]	0.137	0.182
X-ray	pB	0.079	0.000	0.300	0.133	0.175
NMR	pG	0.373[a]	0.383	0.000	0.325	0.371
MD	pG	0.183	0.214	0.373	0.000	0.175
MD	pB	0.226	0.218	0.431	0.193	0.000

(b)		**X-ray PYP_{BL}**	**MD pG**	**MD pR**	**MD pRprot**	**MD pRGln**	**MD pB**
X-ray	PYP	0.000	0.113	0.124	0.155	0.126	0.175
MD	pG	0.185	0.000	0.102	0.169	0.090	0.175
MD	pR	0.183	0.178	0.000	0.153	0.110	0.191
MD	pRprot	0.212	0.223	0.188	0.000	0.131	0.188
MD	pRGln	0.180	0.148	0.163	0.187	0.000	0.174
MD	pB	0.219	0.193	0.234	0.231	0.213	0.000

[a]The values without the N-terminal residues 1–26, as given in Düx et al. (1998), are 0.105 and 0.190, respectively

Comparison of the MD and the X-ray structures

In Fig. 4a the r.m.s. atom-positional deviations of the C_α atoms (solid line) and of all atoms (dotted line) from the corresponding X-ray structure are given with respect to the simulation time. The graph shows an equilibration time of 400–500 ps, after which the average deviation remains about 0.20 nm for all atoms and 0.12 for the C_α atoms throughout the simulation with all residues included. This indicates that the system is sufficiently equilibrated. However, fluctuations are observed throughout the whole simulation time, indicating a sizable backbone flexibility in agreement with the experimental data.

To study the flexibility along the backbone, we compare the r.m.s. atom-positional fluctuations of the C_α atoms for the equilibrated ground state system with the fluctuations of the crystal structure, derived from the experimental *B*-factors (Fig. 5). Figure 5a demonstrates that the flexibility of the protein during the ground state simulation is in very good agreement with the crystallographic data. Regions of high flexibility are found between the residues Ala16 and Ala27, Gly47 and Val57, and around Glu74, Gly86, Met100 and Gly115. For the same regions, increased r.m.s. atom-positional deviations per residue are found between our MD structures and the X-ray structure, as shown in Fig. 3d, except for the N-terminal part in which both structures do not differ much.

Comparison of the MD and the NMR structures

In Fig. 4a the overall r.m.s. atom-positional deviations of the MD structures from the NMR structure with the lowest energy (dashed line) are shown as a function of the simulation time. The deviation is about twice as large as the deviation from the X-ray structure (0.4 nm for all atoms and 0.3 nm for the C_α atoms versus 0.2 nm and 0.12 nm, respectively, for all residues) and does not change during the simulation. However, if the N-terminal region is excluded (see Table 1, footnote) the overall deviations are comparable with the deviations from the X-ray data. This is in agreement with the experimentally observed variation (see above).

We also compared the nuclear Overhauser effect (NOE) distances calculated from our simulation data

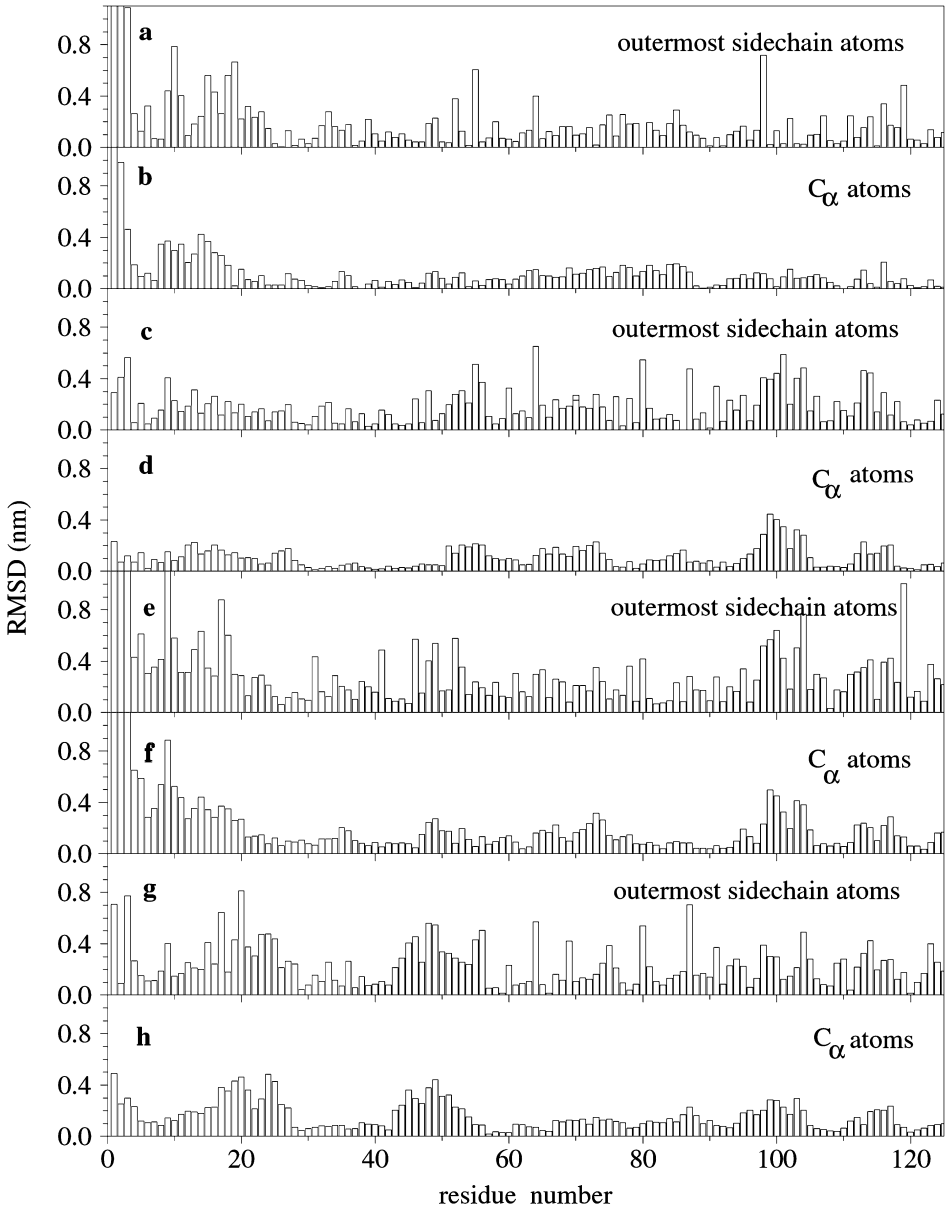

Fig. 3 Root mean-square atom-positional differences along the PYP polypeptide chain for the outermost sidechain atoms and the C_α atoms per residue. (**a**, **b**) R.m.s.d. between pG(X-ray) and pG(NMR); (**c**, **d**) R.m.s.d. between pG(MD) and pG(X-ray); (**e**, **f**) R.m.s.d. between pG(MD) and pG(NMR); (**g**, **h**) R.m.s.d. between pB(MD) and pB(X-ray). For nomenclature, see legend to Table 1

(500–1000 ps) and from the crystal structure with the experimentally determined NOE distance bounds (Düx et al. 1998) (Supplementary material, Table S3). The average violations are all below 0.03 nm for both the crystal and MD data and are therefore well within the overall accuracy of the calculations. In order to ensure that the overall structure is conserved, the location of the single violations above 0.3 nm was investigated. Most of the large violations involve at least one residue which is located at the N-terminus of the backbone (residue numbers 1–26). No large NOE distance restraint violations involving pairs of protein backbone atoms are found, indicating a conservation of the secondary structure.

The same trends were found in Fig. 3e and f, in which are shown the r.m.s. atom-positional deviations for the C_α atoms and the outermost side-chain atoms of the individual residues between the NMR structure and the simulation structure averaged over 500–1000 ps. The largest deviations are again found for the residues Met1-Asp20.

In summary, a pronounced backbone flexibility is observed in both the experimental and our theoretical studies. However, the differences are mainly located in the N-terminal region of the protein and the positional differences in the rest of the protein are below 0.2 nm and the overall backbone structure is well conserved in all three data sets.

Comparison of the pG and pB states

For our comparison of the pG and pB states we examine first their changes in the secondary structures and in the hydrogen bonding networks during the simulations;

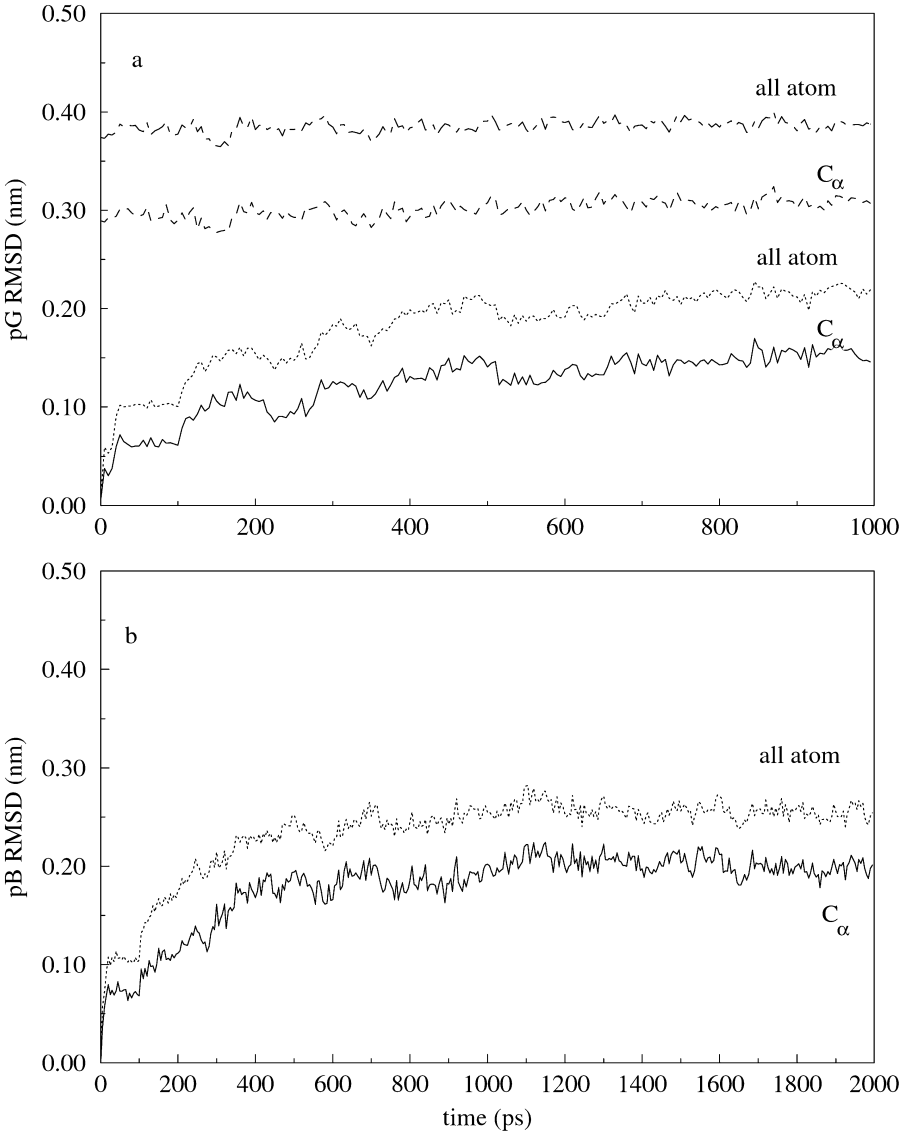

Fig. 4a, b R.m.s. atom-positional differences between the simulation and experimental structures as a function of time for all atoms and the C_α atoms. (**a**) R.m.s.d. during the pG simulation from the pG(X-ray) structure (*solid and dotted lines*) and from the pG(NMR) structure (*dashed and dot-dashed lines*). (**b**) R.m.s.d. during the pB simulation from the pB(X-ray) structure

second, the atom-positional r.m.s. fluctuations around the time-averaged structures and deviations from the starting structures; and finally the overall changes in the shape of the protein.

Figure 6 shows the changes in the secondary structure of the ground state throughout the simulation. Five α-helical regions (dark blue), five β-sheets (red) and several smaller H-bonded turns and bends can be found, which is in agreement with the experimental structures (Borgstahl et al. 1995). The major secondary structure elements remain stable throughout the simulation. The longest stretch of residues without α-helix or β-sheet type of secondary structure is between Ile58 and Ser72, which is the neighbor region of the chromophore (Fig. 2). Between residues Lys60 and Asp65 a periodic folding and unfolding of a hydrogen-bonded turn and helical structure elements can be observed. The α-helix around residue Lys55 turns into a H-bonded turn structure for a few times at the beginning but stabilizes throughout the simulation.

The secondary structure of the signaling state (pB) during the simulation is shown in Fig. 6e. Again the overall secondary structure remains stable throughout the simulation. In the region of the N-terminal cap an additional β-bridge forms after 400 ps between residue Glu2 and Ala27. After 1.5 ns, local changes in the secondary structure can be observed around the chromophore pocket. The α-helix between residue Pro54 and Val57 shows an increasing tendency to turn a H-bonded turn and the β-sheet 2 becomes more and more unstable.

These observations are in agreement with the H-bond populations during the last 500 ps of the simulations, given in Table 2. In this table, only selected H-bond populations are shown, chosen according to their importance for the overall structure retainment and their differences in the ground and signaling state.

Regarding the population of the backbone hydrogen bonds in the ground state around the chromophore pocket, it can be observed that the secondary structure elements at the beginning of this region (α-helix 3) and

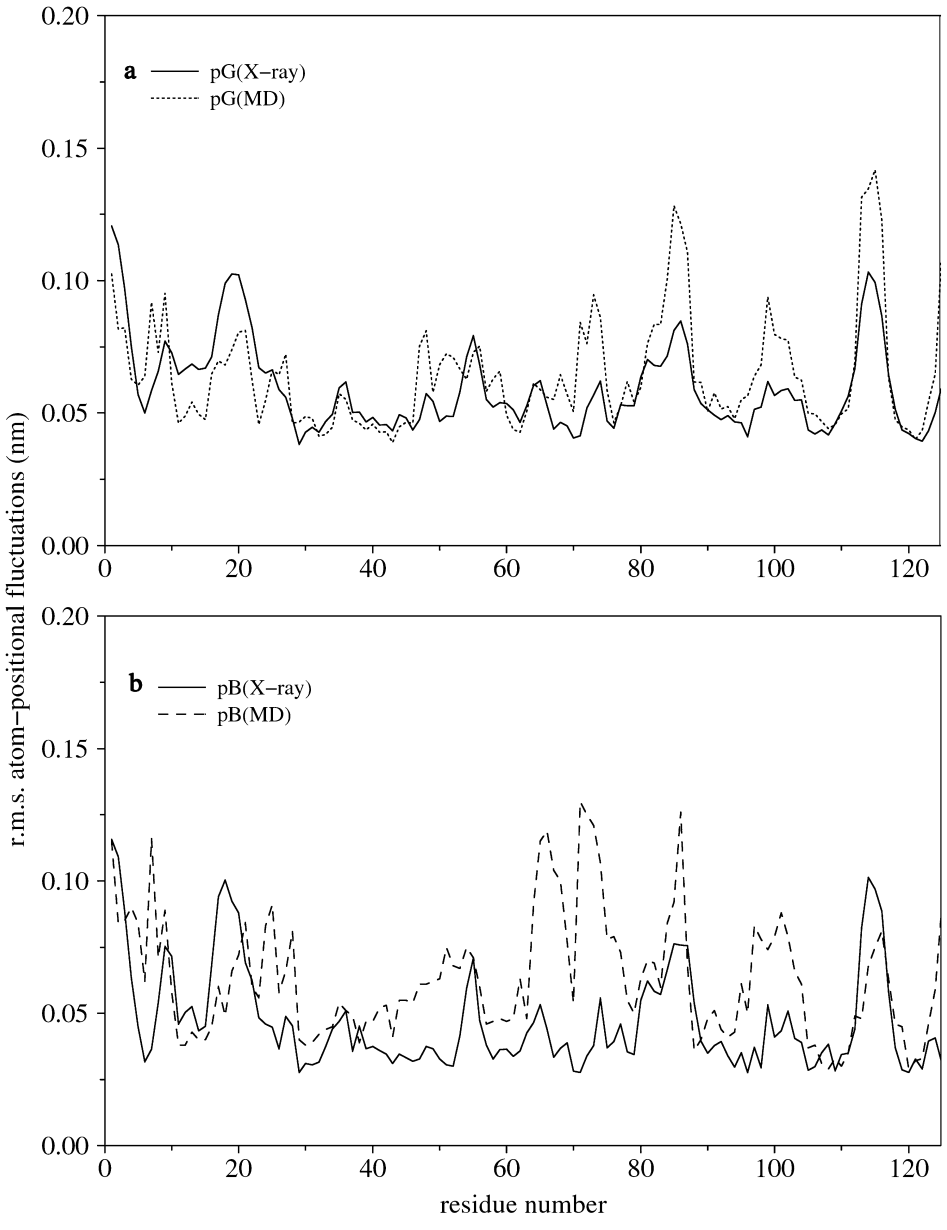

Fig. 5a, b R.m.s. atom-positional fluctuations for the C_α atoms. (**a**) for pG(X-ray) as derived from *B*-factors (*solid line*) and pG(MD) averages over the final 500 ps of the pG simulation (*dotted line*); (**b**) for pB(X-ray) as derived from *B*-factors (*solid line*) and pB(MD) averages over the final 1500 ps of the pB simulation (*dashed line*)

its end (β-sheet 3 and 4) are very stable (Table 2). For residues between these secondary structure elements the H-bond populations vary strongly, indicating an alternation between rigid and flexible parts (see α-helix 4 and the "single bonds" section in Table 2). The backbone hydrogen bonds of α-helix 3 involving residues Gly51 (23%) and Arg52 (18%) are very weak. This is in contrast to the strong H-bond formed by the Arg52 side-chain hydrogen and the Phe98 backbone oxygen (79%; see also Table 3).

In the signaling state the backbone H-bond population is increased for Gly51 and Arg52 (to 82% and 48%), compared with the ground state. The latter is accompanied by a broken side-chain bond to Phe98, due to the open chromophore pocket in the signaling state (0% in contrast to 79% in the ground state; see also Table 3). In addition, the relative populations of the adjacent backbone H-bonds in this region are changed (Ile58-Pro54/Ile58-Lys55), indicating rearrangements in the secondary structure. In addition, a decreased population of the Tyr94-Val105 and Phe96-Thr103 H-bonds of β-sheets 3 and 4 can also be observed. The other secondary structure elements remain very stable. Regarding the side-chain H-bonds in the vicinity of the chromophore, a change in the H-bond network around residues Thr50, Arg52 and Tyr42 can be observed. These observations are in agreement with another MD study of the pB state (Shiozawa et al. 2001). In this study the distance between the chromophore oxygen O1 and the side-chain hydrogens of the Arg52 residue was found to oscillate between 0.3/0.4 nm and 1 nm on a 1 ns time scale. In our simulation we observed the same oscillation on a 500 ps time scale.

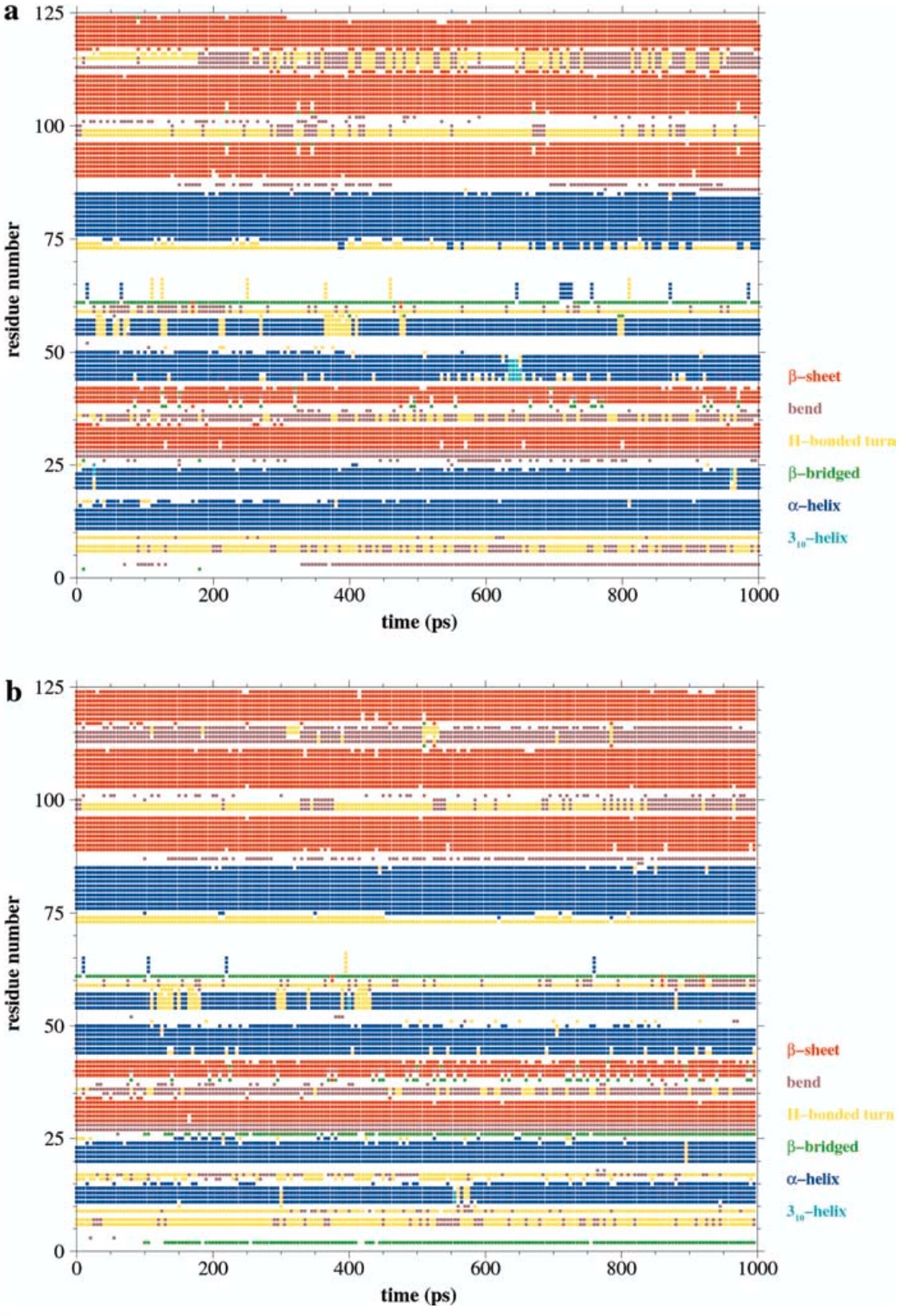

Fig. 6 Secondary structure of PYP as a function of time as determined with the program PROCHECK (Laskowski et al. 1993) for the pG(MD) (**a**), pR(MD) (**b**), pRprot(MD) (**c**), pRGln(MD) (**d**) and pB(MD) (**e**) simulations

Comparing the r.m.s. atom-positional fluctuations of the C_α atoms, averaged over the last 500 ps (pG state) or 1500 ps (pB state) of these two simulations, as shown in Fig. 5, drastically increased fluctuations can

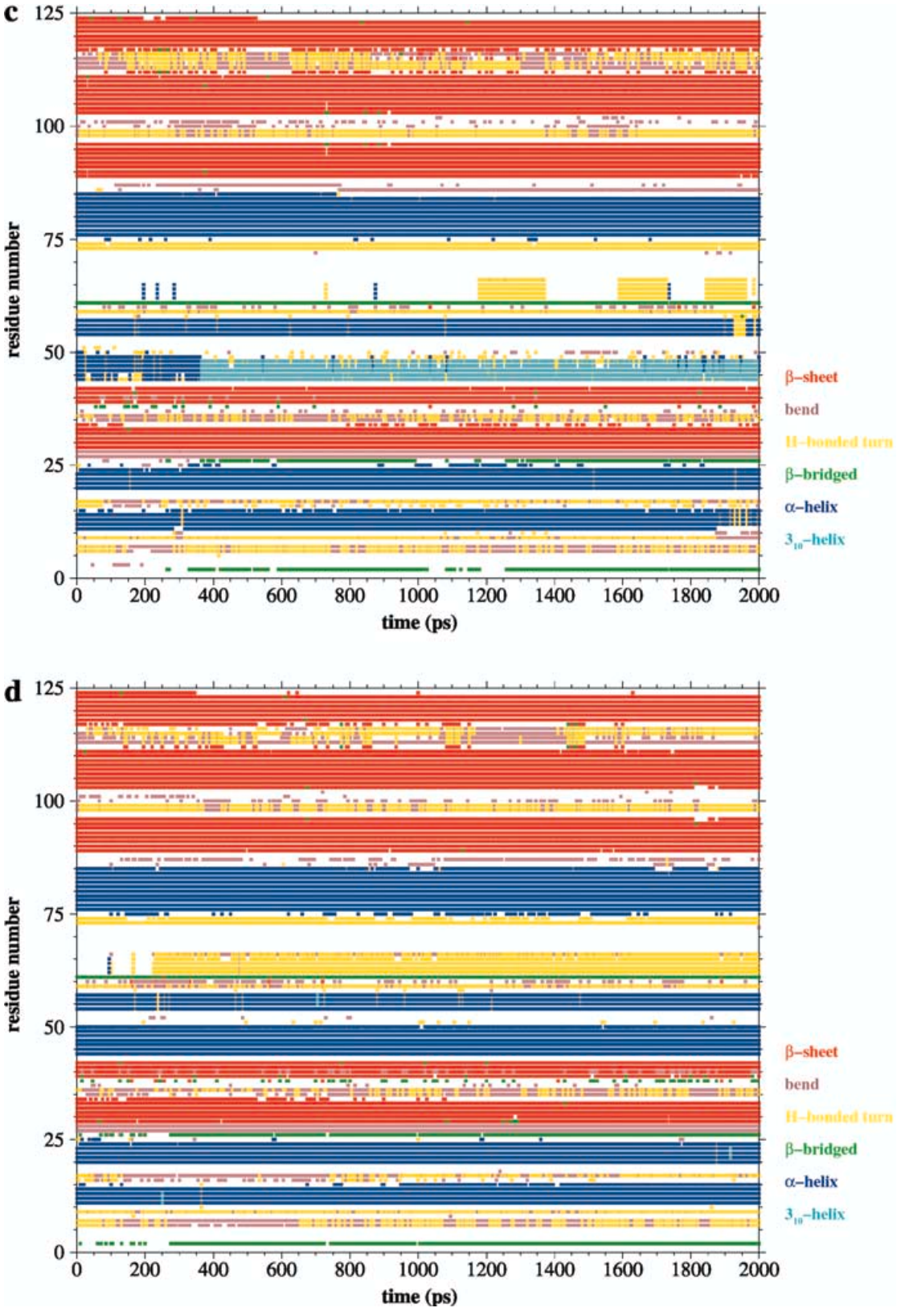

Fig. 6 (Contd.)

be observed for the signaling state between the residues around Val66 and Ser72, which is another indication for structural rearrangements around the chromophore pocket.

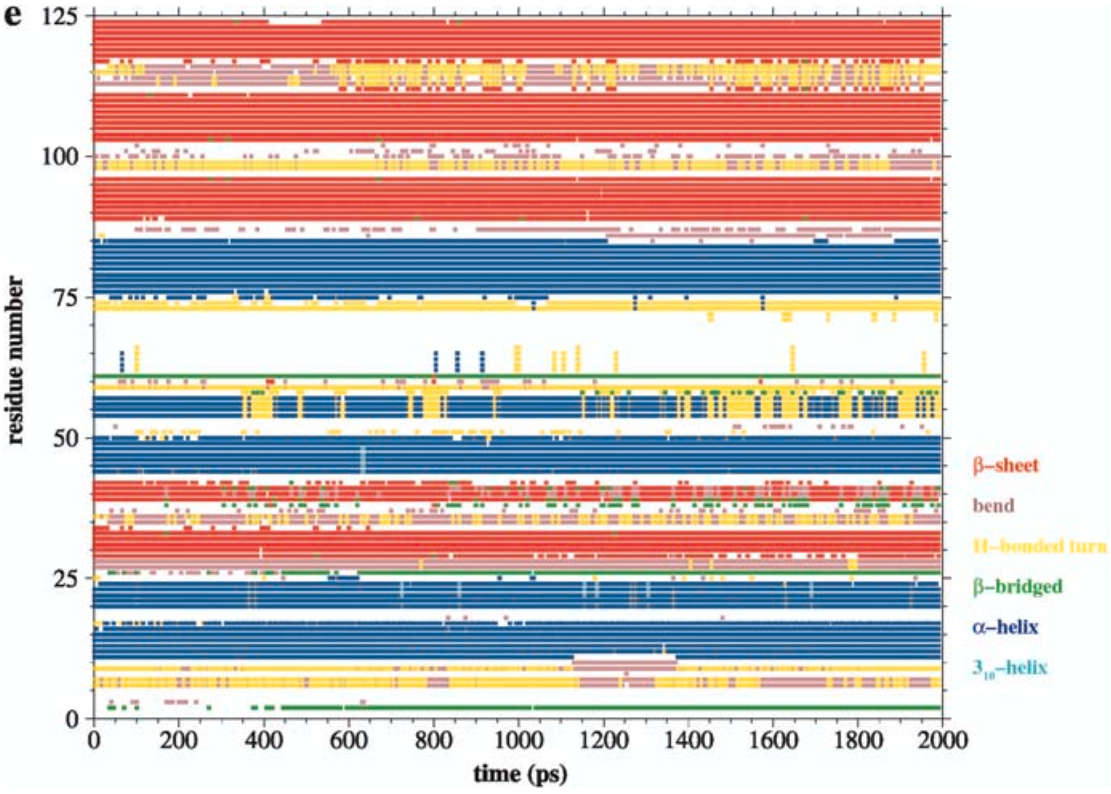

Fig. 6 (Contd.)

Additional major changes in hydrogen bonding were found in the region around the N-terminal cap of the protein. This region forms only very few H-bonds with the remainder of the protein and is therefore relatively flexible with respect to the rest of the structure. In the ground state there is only one backbone H-bond between the N-terminal cap and the rest of the protein, from residue Ala45 to Asp24, in addition to several side-chain H-bonds between the residues Asn43-Leu23, Asn43-Phe28 and Ala44-Asp24. However, these are all located within the a very localized region (residues Leu23 to Phe28) of the N-terminal cap, connecting only its end with the rest of the protein, thus leaving its beginning part rather flexible.

The H-bonding populations of the signaling state in this region show that none of the hydrogen bonds connecting the N-terminal cap with the remaining protein are retained. However, a new H-bond was formed between the backbone atoms of residues Leu113 and Glu12, interestingly connecting the previously unconnected part of the N-terminal cap to the main part of the protein. The secondary structure elements (α-helices 1 and 2) within the N-terminal cap remain stable.

In Fig. 3c and d (ground state), and Fig. 3g and h (signaling state), respectively, the r.m.s. atom-positional differences of the C_α atoms and the outermost side-chain atoms of the amino acid side chains between the averaged MD structure and the corresponding crystal structure are given. Regarding the ground state data, in the surroundings of the active site the smallest deviations are found from residue Ala30 to Thr50 (around 0.05 nm) and at the end of the chromophore pocket between the residues Tyr76 and Thr95, whereas the deviations of the backbone around the chromophore (residues Gly51-Phe75) are more pronounced (around 0.15 nm). In addition, very small deviations can be found at the end of the protein around residue Lys110 and Val120-Val125. The region where the structures differ most is around residue Met100.

For the signaling state (pB) the average deviations (Fig. 3g and h) are larger than for the ground state, which is in agreement with an increased overall r.m.s. positional deviation of 0.18 nm (C_α atoms) given in Table 1. A comparably high flexibility can be found in the pB state for stable ground state regions, especially around α-helix 3 (Asn43-Arg52) and the region around residue Asp20 (residues Asp10-Phe28 and Asn43-Glu56). Because of the retained stability of α-helix 3 in the pB state (Table 2), the increased deviation in this region indicates a collective movement of the helix.

To study the effect of the above observations on the shape of PYP, we compare the backbone conformations of the ground state and of the signaling state after 1 ns (pG, red) and 2 ns (pB, blue) of simulation time (Supplementary material, Fig. S1). The chromophore pocket is shown on the left side and the N-terminal cap to the right. Although no dramatic changes in the overall structure can be expected after a simulation time of 2 ns, some changes can be observed. Dividing the structures into an "upper" region consisting of residues Pro75-Val125 (α-helix 5 and β-sheets 3, 4 and 5) and a "lower"

Table 2 Percentage of hydrogen bonding in the X-ray crystal structure pG(X-ray) and in the final 500 ps periods of the pG(MD) and pB(MD) simulations. A hydrogen bond is assumed to exist if the hydrogen-acceptor distance is smaller than 0.30 nm and for the backbone hydrogen bonds the donor-hydrogen-acceptor angle is greater than 135°

(a) Backbone hydrogen bonds around the chromophore pocket			
	pG(X-ray)	**pG(MD)**	**pB(MD)**
α-helix 3			
Gly47-Asn43	100	92	78
Asp48-Ala44	100	75	93
Ile49-Ala45	100	90	92
Thr50-Glu46	100	78	90
Gly51-Gly47	0	23	82
Arg52-Gly47	0	18	48
α-helix 4			
Val57-Asp53	100	96	92
Ile58-Pro54	100	84	22
Ile58-Lys55	100	17	70
Lys60-Val57	100	52	42
Single H-bonds			
Asp65-Asn61	100	22	48
Val66-Asn61	100	84	88
Ala67-Phe62	100	70	84
Thr70-Ala67	100	40	37
Asp71-Pro68	100	32	59
Phe75-Ser72	100	54	40
Tyr76-Thr70	100	97	87
Gly77-Ser72	100	99	93
α-helix 5			
Lys78-Pro73	100	85	93
Phe79-Phe75	100	96	98
Lys80-Tyr76	100	99	99
Glu81-Gly77	100	96	93
Gly82-Phe78	100	82	77
Val83-Phe79	100	98	92
Ala84-Lys80	100	97	96
Ser85-Glu81	100	95	90
β-sheets 3 and 4			
Thr90-Met109	100	93	91
Phe92-Val107	100	96	98
Tyr94-Val105	100	67	53
Phe96-Thr103	100	94	64
(b) Hydrogen bonds in other regions and involving side chains			
	pG(X-ray)	**pG(MD)**	**pB(MD)**
Glu2-Gly25	100	75	84
Ala27-Glu2	0	0	90
Leu23-Asp19	100	97	98
Asp24-Asp20	100	91	86
Gly25-Gln22	100	48	37
Ala30-Phe28	0	0	86
Ala45-Asp24	100	47	0
Gln32-Gln41	100	92	90
Leu40-Gln32	100	78	88
Leu113-Glu12	0	0	92
Tyr118-Leu33	100	96	88
Val120-Ile31	100	99	98
Val122-Gly29	100	95	98
Gly59-Ile39	100	94	90
Side chain H-bonds			
Gln41(HE21)-Asp20(O)	0	0	66
Arg52(HH21)-Tyr98(O)	100	79	0
Asn43(HD22)-Leu23(O)	100	98	0
Asn43(HD22)-Phe28(O)	100	98	0
Ala44(H)-Asp24(OD1)	100	60	0

region with the residues Met1-Ser72 (α-helices 1–3 and β-sheets 1 and 2), a relative movement of the lower part with respect to the upper region to the left can be observed. In addition, structural changes in β-sheet 2 and a movement of the N-terminal cap can be identified. The α-helix 3 moves towards the upper β-sheets 3 and 4 around residue Met100. The reason for this is most likely the broken H-bonding network in the chromophore pocket, especially the weakened Arg52-Phe98 hydrogen bond, which forms a rather rigid connection between the two secondary structures in the ground state.

Comparing the solvent accessible surface areas of the ground and signaling states (Supplementary material, Fig. S2), a local change in the shape can be observed on the lower part and the ''gap'' between the upper and lower regions around the chromophore pocket closes. This is accompanied by a change in the distribution of the surface groups, and the Cys69 sulfur atom becomes exposed in the chromophore region.

Dynamics of the chromophore after photoexcitation

Upon photoexcitation, a *trans* to *cis* isomerization of the chromophore double bond between C7 and C8 (Fig. 2) is observed (Kort et al. 1996). This is accomplished by a 180° rotation of the C9 = O2 carbonyl group, close to the double bond (Genick et al. 1998; Ren et al. 2001). During the following relaxation towards the pB state, the C9 = O2 carbonyl group moves back into its original position, the chromophore pocket opens towards the solvent and the chromophore becomes solvent exposed (Genick et al. 1997b; Ren et al. 2001).

As mentioned in the Introduction, there is experimental evidence that the protonation states of the chromophore and its surrounding residues are of key importance for the transition of the pR to the pB state. In addition, mutation and FTIR experiments have highlighted the crucial role of the residue Glu46, which forms a hydrogen bond with the phenoxyl oxygen of the chromophore. Proton transfer from Glu46 to pCA69 has also been suggested. In an attempt to elucidate the role of Glu46 and its protonation states, we performed three MD simulations starting from the PYP_{BL} structure, the first with the chromophore pCA unprotonated and Glu46 protonated (pR), the second one with pCA protonated at O1 and Gly46 unprotonated (pRprot), and the third one with pCA unprotonated and Glu46 exchanged for Gln46 (pRGln).

In Fig. 6b–d the changes in the secondary structure during the pR, pRprot and pRGln simulations are shown. All three simulations show an overall retainment of the secondary structure, indicating stable simulation conditions. However, local changes around the chromophore pocket are observed for the pRprot and pRGln simulations, although not for pR. During the simulation of pRprot the α-helix 3 turns into a 3_{10}-helix after 350 ps and after 1150 ps a H-bonded turns starts to form between the residues Phe63 and Val66. In the pRGln simulation the formation of the same H-bonded turn as for the pRprot simulation can be observed after

250 ps, which stays stable throughout the rest of the simulation.

In Table 3 the H-bond populations within the chromophore pocket are specified. During the pR simulation, most of the ground state H-bonds are retained, except for the bond between the backbone hydrogen atom of Cys69 and the O2 atom of pCA, which is broken because of the *trans-cis* isomerization of pCA. The hydrogen bonding between the chromophore O1 and Glu46 is strengthened in pR compared with the ground state pG. This is accompanied by weakened Thr50(HG1)-Tyr42(OH) and Arg52(HH21)-Tyr98(O) hydrogen bonds. The latter is important for the closing of the chromophore pocket and the retainment of the overall structure in this area. During the pRprot simulation the hydrogen bond between the chromophore H1 atom and Glu46, Tyr42 and Thr50 is much weaker than in pR and pG and the Thr50(HG1)-Tyr42(OH) and Arg52(HH12)-Thr50(O) hydrogen bonds do break. In addition, an increase in the H-bond population for the interaction of the chromophore with Arg52 can be seen. The population of the hydrogen bond between the O2 atom of pCA and the backbone hydrogen atom of Cys69 is 68%, indicating a reformation of this hydrogen bond during the pRprot simulation. Different changes in the H-bond patterns can be observed for pRGln. The Cys69(H)-pCA69(O2), the Gln46(HE2)-pCA69(O1) and the Thr50(HG1)-pCA69(O1) hydrogen bonds are broken, whereas all three hydrogen bonds involving Arg52 have populations of nearly 100%.

In Table 4 we compare the torsional angles of the X-ray structures of pG and PYP_{BL} with the average torsional angles during the final 500 ps of the pG and pR simulations and during the final 1500 ps of the pRprot, pRGln and pB simulations. Because the pR values are taken from the 3PYP structure, which was

Table 3 Percentage of hydrogen bonding in the X-ray crystal structures pG(X-ray) and pB(X-ray) and in the final 500 ps periods of the pG, pR and pB and the final 1500 ps periods of the pRprot and pRGln simulations. A hydrogen bond is assumed to exist if the hydrogen-acceptor distance if smaller than 0.30 nm

Atom pair	X-ray		MD	MD	MD	MD	MD
	pG	pB	pG	pR	pRprot[a]	pRGln	pB
Cys69(H)-pCA69(O2)	100	100	28	0	68	0	23
Glu46(HE2)-pCA69(O1)	100	0	64	98	64	0	0
Tyr42(HH)-pCA69(O1)	100	0	100	100	62	100	0
Thr50(HG1)-pCA69(O1)	100	0	100	98	19	3	0
Thr50(HG1)-Tyr42(OH)	100	100	85	63	0	100	23
Arg52(HH12)-Thr50(O)	100	0	51	56	0	99	0
Arg52(HH21)-Tyr98(O)	100	0	79	20	27	100	0
Arg52(HH12)-pCA69(O1)	0	100	5	9	40	94	0
Tyr50(H)-Glu46(O)	100	100	78	86	0	73	90

[a]Owing to the protonation of pCA at O1, the donor/acceptor atoms are exchanged for the hydrogen bonds involving phenoxyl group of pCA

Table 4 Torsional angles for the residues which are involved in the pR to pB transition. pG(X-ray): crystal structure of the ground state (PDB code 2PHY); PYP_{BL}(X-ray): crystal structure shortly after the photoexcitation (PDB code 2PYP); pG(MD): average torsional angle (over period 500–1000 ps) in the pG simulation; pR(MD): average torsional angle (over period 500–1000 ps) in the pR simulation; pRprot(MD): average torsional angle (over period 500–2000 ps) in the pRprot simulation; pRGln(MD): average torsional angle (over period 500–2000 ps) in the pRGln simulation; pB(MD): average torsional angle (over period 500–2000 ps) in the pB simulation

Residue	Torsional angle	X-ray		MD	MD	MD	MD	MD
		pG	pR	pG	pR	pRprot	pRGln	pB
Tyr42	χ_1	–169	–158	–173	–171	–168	–163	–167
	χ_2	–81	–95	–85	–88	–95	–109	–111
Glu46	χ_1	–175	–178	–163	–169	–166	–166	–72
	χ_2	64	70	66	65	–90	66	–51
	χ_3	–172	178	–132	–160	112	–153	5
Arg52	χ_1	–84	–80	–102	–85	–79	–141	–69
	χ_2	64	57	104	141	168	76	–101
	χ_3	178	–87	–98	179	168	65	178
	χ_4	–173	–164	149	119	84	–116	–146
pCA69	χ_1	80	18	70	64	–66	61	146
	χ_2	–82	67	–119	–137	100	113	–88
	χ_3	174	–127	–164	–155	–180	109	162
	χ_4	176	–123	146	–28	–155	88	148
	χ_5	–177	–72	–178	1	4	3	–1
	χ_6	179	–142	–102	–141	–64	–65	–89
Phe75	χ_1	–165	–167	–160	–113	–88	–130	–113
	χ_2	–52	–44	–66	–88	–83	124	–134
Phe96	χ_1	–66	–73	–85	–78	–85	–90	–89
	χ_2	–20	7	21	–75	40	19	50
Tyr98	χ_1	–178	–180	–172	–105	–162	–172	180
	χ_2	61	70	94	23	69	58	72

trapped directly after the photoexcitation, the chromophore has not yet reached the minimum *cis* conformation (see Introduction) in this structure. This can explain why, during the pR, pRprot and pRGln simulations, the torsional angles for the chromophore differ considerably from the PYP_{BL} (X-ray) values. The torsional angles are mostly retained for the surrounding residues Tyr42, Glu46, Phe75, Phe96 and Tyr98 and the major changes are seen for Arg52 and pCA69. The torsional angles of the chromophore in the ground state pG(MD) stay close to the values of the pG(X-ray) structure. The same can be observed for the pB state, compared with the torsional angles for the chromophore in pB(X-ray), which are 89°, –77°, 169°, 158°, –19° and –38°, respectively (not given in Table 4). The major difference is the χ_1 torsional angle, which is 146° in the pB simulation. This difference may be caused by the strong backbone movement of the signaling state in this region (see previous discussion); the pB(MD) values for this torsional angle vary from 52° to 218° in the simulation and have a r.m.s. fluctuation of 38°.

To gain a better impression on the effect of the data discussed above, we provide snapshots of the structures of the pR, pRprot and pRGln systems during the simulations in the Supplementary material. Snapshots were taken whenever an important movement was observed. We included the key residues Tyr42, Thr50, Glu46, Arg52, pCA69, Cys69, Phe75, Phe96 and Phe98 in the pictures. In addition, we show the X-ray structures of pG and pB and the final configurations of our pR, pRprot and pRGln trajectories in Fig. 2c–f. For pR the starting, intermediate and final structures are very similar, although the C9=O2 group of pCA moves out of the Phe75/Phe96 pocket. This is due to the relaxation of the PYP_{BL} state into a stable intermediate at room temperature, but no other large changes are observed. This is in agreement with the results of Ren et al. (2001), which show that the structures measured within the first few nanoseconds after the photoexcitation are very similar to the 3PYP structure. However, if the chromophore is protonated, as in the pRprot simulation, the C9=O2 group moves out of the Phe75/Phe96 pocket much faster (after 165 ps) and reforms the Cys69-pCA69 hydrogen bond. During the first nanosecond, pCA69(OH) forms a hydrogen bond with Glu46(OE), as does Tyr42(OH). After 1160 ps the pCA69(HO)-Glu46(OE) hydrogen bond breaks and pCA(HO) forms a hydrogen bond with Tyr42(O), while Tyr42(HO) continues to be hydrogen bonded to Glu46(OE). This leads to a movement of the chromophore, the breakage of the Cys69(NH)-pCA69(O2) hydrogen bond (after 1185 ps), and some rearrangements in the regions around the residues Tyr42 and Glu46. After 1605 ps the Cys69(NH)-pCA69(O2) hydrogen bond reforms and a stabilization is observed, resulting in no further large movements until the end of the simulation.

The conformational changes in the pRGln simulation differ drastically from the pR and pRprot ones. The hydrogen bond between the pCA(O1) and Gln46(NH) atoms is less strong than with Glu46(NH) and thus the phenoxyl group of the chromophore is relatively mobile. Therefore, the strain which is put on the chromophore upon the photoexcitation and the rotation of the C9=O2 group in the Phe75/Phe96 pocket is not released by the movement of the C9=O2 group back out of this pocket, but by a movement of the phenoxyl group (after 140 ps). This leads to a rotation of Arg52 and an adaption of its surroundings after 500 ps by a movement of Tyr98. Owing to this movement, the pocket opens up between the residues Tyr98 and Phe75 and after 1 ns water moves into the pocket and surrounds the chromophore. This might lead to the protonation of the chromophore through the solvent.

Discussion

Comparison of the ground state structures

The comparison of the average r.m.s. deviations between the NMR, X-ray and time-averaged MD structures show a difference of about 0.3 nm for the C_α atoms, between the NMR structure on the one hand and the X-ray and average MD structures on the other (Table 1), if all residues are included in the calculation of the r.m.s.d. The deviations between the X-ray and the MD structure are much smaller (0.137 nm for the C_α atoms and 0.183 nm for all atoms). However, if the residues 1–26 (N-terminal cap) are excluded from the calculation, the r.m.s. deviations are within 0.2 nm for all three structures. This agrees with the data shown in Fig. 3, where especially large deviations can be observed at the N-terminus of the protein backbone from residue Met1 to Asp20. In addition, when comparing the NOE distance bounds derived in the NMR study with distances calculated for our simulation and the X-ray structure, most of the larger violations do involve residues of the N-terminal region. Therefore, this region differs most in the three structures. The overall secondary structure was retained in all three data sets. These results suggest that PYP in its ground state has a high local backbone flexibility, a fact which is in agreement with several experimental studies (Düx et al. 1998; Rubinstenn et al. 1998; van Aalten et al. 2000).

Comparison of the pG and pB states

As mentioned above, PYP is a prototype for the PAS domain superfamily, which includes diverse signaling and sensing proteins. Sequence alignment studies on the PYP/PAS family indicate that three regions are involved in the signal transduction. First, the chromophore pocket region of about 1 nm radius around Arg52; second, the loop of residues Thr95-Thr103 which closes the chromophore pocket on the opposite side of Arg52;

and third, the residues Ala44 and Ala45 which are part of α-helix 3. The Thr95-Thr103 loop is considered to play a role in the recognition specificity for the PAS dimerization because of the low sequence homology among the PAS domains in this area (Pellequer et al. 1998).

Comparing the secondary structure, the hydrogen bonding network and the r.m.s. atom-positional fluctuations and deviations during the simulations of the pG and pB states, we identified two major regions of differences: the region around the chromophore pocket (approx. residues 40–100) and the area of the N-terminal cap (residues Met1 to Phe28), which are connected through α-helix 3.

In the region around the chromophore pocket, local changes can be observed after 1.5 ns, mainly between residue Leu40 and Phe75 in the pB simulation. Studying the backbone H-bonding network in this region, it can also be observed that the secondary structure elements surrounding the chromophore pocket are very stable (α-helix 3 and 5 and the β-sheets 3 and 4). Between these elements the populations of the backbone hydrogen bonds vary strongly and differ in the pG and pB states, indicating local structural rearrangements. Our data show that major differences in the backbone H-bonding occur mainly in the region from residue Leu40 to Thr70 and around residue 100. Around the latter we observe a decreased H-bonding population for the Tyr94-Val105 and Phe96-Thr103 hydrogen bonds of β-sheets 3 and 4 (Table 2) and increased r.m.s. atom-positional fluctuations. The β-sheet 2 starts to become unstable, turning into bends and β-bridges (Fig. 6e). These observations are in agreement with an increase in the r.m.s. atom-positional fluctuations in these regions in the pB state compared with the pG state (Fig. 5). Both regions were identified to be important for the signal transduction in PAS proteins (Pellequer et al. 1998) and were also found to be very flexible in another MD study (Shiozawa et al. 2001). In addition, in Fig. 3g and h the regions between residues Asp20 and Ala30 and Tyr42 and Arg52, which have very small r.m.s. deviations in the pG state (Fig. 3c and d), do show very large deviations up to 0.4 nm in the pB state, indicating some significant movements. This region comprises the β-sheet 1, the α-helix 3 and several hydrogen bonds with the N-terminal cap in the pG state. Because the α-helix 3 itself was found to be very stable, this indicates a collective movement of the whole helix, which is in agreement with the sequence alignment data.

Regarding the N-terminal cap, the H-bonding network between this region and the rest of the protein was found to be different from that of the pG state. All hydrogen bonds with this region which are present in the pG state are broken in the pB simulation and new backbone hydrogen bonds are formed with the N-terminal cap (Ala30-Phe28, Leu113-Glu12, Glu41-Asp20; Table 2). Within the N-terminal cap itself the hydrogen bonding and secondary structure remains stable. Therefore the high r.m.s. atom-positional fluctuations in this region are most likely due to a collective movement of the cap with respect to the rest of the protein. The same region was also found to move considerably in a study of the pB state by solution NMR (Rubinstenn et al. 1998). This may be connected to its function to protect the central hydrophobic β-sheet from the solvent. Experimental studies have shown an increase in the hydrophobic area exposed to the solvent in the signaling state (Hoff et al. 1999; Hendriks et al. 2002), which could have its cause in a structural shift of the N-terminal cap.

In the Supplementary material we show the overall differences in the protein backbone structure and shape. The major movement can be observed for the α-helix 3 and the N-terminus. The gap between the α-helix 3 and the N-terminus is increased in the pB state, which can be explained by the broken ground-state hydrogen bonding (Table 2). These changes affect the overall shape of the protein and do cause changes in the distribution of the solvent exposed groups, which can be a prerequisite for the signal transduction (Hendriks et al. 1999, 2002).

The dynamics of the chromophore after photoexcitation

Experimental studies by optical and FTIR spectroscopy and theoretical work, including the mutant Gln46 (E46Q), have shown that the protonation state of the chromophore and Glu46 is of crucial importance for the relaxation of the protein after its photoexcitation. Through our simulations with the chromophore in its unprotonated and protonated form and of the pRGln mutant, we intended to gain a better understanding of the effect of these changes on the transition mechanism from pR to pB.

Our simulation data (Tables 3 and 4 and Supplementary material, Fig. S3) show no significant rearrangements in the pR simulation, except for the relaxation around the *cis* double bond in the chromophore, which is strained in the PYP_{BL} structure and relaxation is expected. We found an increased strength of the pCA69-Glu46 hydrogen bond compared with the ground state structure, which restricts the movement of the chromophore. This is in agreement with a series of time-resolved diffraction structures, which are structurally very close to the 3PYP structure for at least 5–10 ns after the photoexcitation, except for the release of the strain around the chromophore's *cis* double bond (Ren et al. 2001).

In contrast, during our pRprot simulation the protonation of pCA and deprotonation of Glu46 leads to a weakened pCA-Glu46 hydrogen bond and to a continuous movement of the chromophore and the surrounding pocket throughout the simulation, ending in a broken pCA(H1)-Glu46(OE2) and a reformed Cys69(H)-pCA(O2) hydrogen bond. This is in agreement with the proposition that a proton transfer from Glu46 to pCA is necessary to "release" the strain put upon the chromophore through the photoisomerization.

In the pRGln simulation the weak pCA(HH)-Gln46(NE2) bond (compared to pR) leads to a different

relaxation mechanism of the chromophore. Instead of a "strain release" through a movement of the C9 = O2 bond, as in pR (and pRprot), the position of the phenoxyl group changes. Owing to this, the phenoxyl oxygen anion forms two new very stable hydrogen bonds with Tyr42 and Arg52, leading to the opening of the chromophore pocket between Tyr98 and Phe75. This allows solvent molecules to enter and interact with the chromophore, which might lead to the protonation of the chromophore by the solvent. This process is completed within 1000 ps. During the second nanosecond of the pRGln simulation the situation remains stable. This mechanism can explain the higher rate constant for the pR to pB transition found for the pRGln mutant compared to the native protein.

The simulations demonstrate the crucial importance of Glu46 and its hydrogen bond to the chromophore for the specific reaction mechanism and reinforces the hypothesis of the protonation of the chromophore as the rate-determining step in the pR to pB relaxation mechanism.

Conclusions

Comparing our simulation results with two different sets of experimental structures obtained by X-ray crystallography and solution NMR, we found that the largest deviations between the different structures were localized at the N-terminal region of the protein. In addition, a high backbone flexibility could be observed at the region around the chromophore pocket, indicating that these two regions are of importance for the structural changes during the photocycle.

This was confirmed by comparing the backbone structures of the ground and signaling state of PYP. Pronounced structural differences were observed to occur around the region of the chromophore pocket, owing to the isomerization and protonation of the chromophore, and its exposure to the solvent though the opened pocket. This is accompanied by local rearrangements of the backbone structure in this area, especially around the residues 50 and 100, causing a shift in the position of α-helix 3, which then leads to changes in the position of the N-terminal cap and its relative position with respect to the rest of the protein. Owing to these structural rearrangements, an overall change in the shape and distribution of the solvent-exposed groups can be observed, which may be a prerequisite for the signaling process. These differences are in agreement with the observations by solution NMR and the results of sequence alignment studies of PYP as a prototype for the PAS domain superfamily (Düx et al. 1998; Pellequer et al. 1998; Rubinstenn et al. 1998). Recent studies also show that local changes in the chromophore pocket, such as charge formation due to the deprotonation of Glu46 (Xie et al. 2001) or changes in the hydrogen-bonding pattern (Ren et al. 2001), can lead to the global structural changes necessary for the signaling process.

Several experimental studies have highlighted the importance of the residue Glu46 and the protonation state of the chromophore to the pR to pB transition after the photoexcitation of the chromophore. Our results confirm the important role of the Glu46(HE2)-pCA(O1) hydrogen bond. This hydrogen bond efficiently restrains the phenoxyl region of the chromophore very closely to its ground state position, thus preventing larger movements immediately after the photoexcitation. Once the chromophore is protonated (pRprot), or the hydrogen bond is considerably weakened as in the pRGln mutant, these larger movements take place, leading to rearrangements of the chromophore and the surrounding residues. These movements differ considerably for the pRprot and pRGln systems. In the former, the strain put upon the chromophore due to the photoisomerization is released through the rotation of its C9 = O2 group. In the latter, it is released through the movement of its phenoxyl group, thus enabling the opening of the chromophore pocket without former protonation of the chromophore and the intrusion of water into the pocket within simulation time. These results are in agreement with the higher rate constant for the pR to pB state transition observed for the pRGln mutant and demonstrate the strong restraining effect the hydrogen bond with Glu46 exerts upon chromophore motion.

Acknowledgements We thank Petra Düx and Rob Kaptein for providing us with the NOE data concerning PYP, and Xavier Daura for his help with the simulation setup and data analysis.

References

Baca M, Borgstahl GEO, Boissinot M, Burke PM, Williams DR, Slater KA, Getzoff ED (1994) Complete chemical structure of photoactive yellow protein: novel thioester-linked 4-hydroxycinnamyl chromophore and photocycle chemistry. Biochemistry 33:14369–14377

Berendsen HJC, Postma JPM, van Gunsteren WF, Hermans J (1981) Interaction models for water in relation to protein hydration. In: Pullman B (ed) Intermolecular forces. Reidel, Dordrecht, pp 331–342

Berendsen HJC, Postma JPM, van Gunsteren WF, DiNola A, Haak JR (1984) Molecular-dynamics with coupling to an external bath. J Phys Chem 81:3684–3690

Borgstahl GEO, Williams DR, Getzoff ED (1995) 1.4 Angstrom structure of photoactive yellow protein, a cytosolic photoreceptor: unusual fold, active site, and chromophore. Biochemistry 34:6278–6287

Demchuk E, Genick UK, Woo TTW, Getzoff ED, Bashford D (2000) Protonation states and pH titration in the photocycle of photoactive yellow protein. Biochemistry 39:1100–1113

Düx P, Rubinstenn G, Vuister GW, Boelens R, Mulder FAA, Hard K, Hoff WD, Kroon AR, Crielaard W, Hellingwerf KJ, Kaptein R (1998) Solution structure and backbone dynamics of the photoactive yellow protein. Biochemistry 37:12689–12699

Genick UK, Borgstahl GEO, Ng K, Ren Z, Pradervand C, Burke PM, Srajer V, Teng TY, Schildkamp W, McRee DE, Moffat K, Getzoff ED (1997a) Structure of a protein photocycle intermediate by millisecond time-resolved crystallography. Science 275:1471–1475

Genick UK, Devanathan S, Meyer TE, Canestrelli IL, Williams E, Cusanovich MA, Tollin G, Getzoff ED (1997b) Active site

mutants implicate key residues for control of color and light cycle kinetics of photoactive yellow protein. Biochemistry 36:8–14

Genick UK, Soltis SM, Kuhn P, Canestrelli IL, Getzoff ED (1998) Structure at 0.85 angstrom resolution of an early protein photocycle intermediate. Nature 392:206–209

He Z, Martin CH, Birge R, Freed KF (2000) Theoretical studies on excited states of a phenolate anion in the environment of photoactive yellow protein. J Phys Chem A 104:2939–2952

Hendriks J, Hoff WD, Crielaard W, Hellingwerf KJ (1999) Protonation-deprotonation reactions triggered by photoactivation of photoactive yellow protein from *Ectothiorhodospira halophila*. J Biol Chem 274:17655–17660

Hendriks J, Gensch T, Hviid L, van der Horst MA, Hellingwerf KJ, van Thor JJ (2002) Transient exposure of hydrophobic surface in the photoactive yellow protein monitored with Nile red. Biophys J 82:17655–17660

Hoff WD, Düx P, Hard K, Devreese B, Nugteren-Roodzant IM, Crielaard W, Boelens R, Kaptein R, Van Beeumen J, Hellingwerf KJ (1994a) Thiol ester-linked *p*-coumaric acid as a new photoactive prosthetic group in a protein with rhodopsin-like photochemistry. Biochemistry 33:13959–13962

Hoff WD, van Stokkum IHM, van Ramesdonk HJ, van Brederode ME, Brouwer AM, Fitch JC, Meyer TE, van Grondelle R, Hellingwerf KJ (1994b) Measurement and global analysis of the absorbency changes in the photocycle of the photoactive yellow protein from *Ectothiorhodospira halophila*. Biophys J 67:1691–1705

Hoff WD, Xie A, Van Stokkum IHM, Tang X, Gural J, Kroon AR, Hellingwerf KJ (1999) Global conformational changes upon receptor stimulation in photoactive yellow protein. Biochemistry 38:1009–1017

Imamoto Y, Kataoka M, Tokunaga F (1996) Photoreaction cycle of photoactive yellow protein from *Ectothiorhodospira halophila* studied by low-temperature spectroscopy. Biochemistry 35:14047–14053

Imamoto Y, Mihara K, Hisatomi O, Kataoka M, Tokunaga F, Bojkova N, Yoshihara K (1997) Evidence for proton transfer from Glu-46 to the chromophore during the photocycle of photoactive yellow protein. J Biol Chem 272:12905–12908

Kort R, Vonk H, Xu X, Hoff WD, Crielaard W, Hellingwerf KJ (1996) Evidence for *trans-cis* isomerization of the *p*-coumaric acid chromophore as the photochemical basis of the photocycle of photoactive yellow protein. FEBS Lett 382:73–78

Laskowski RA, MacArthur MW, Moss DS, Thornton JM (1993) PROCHECK: a program to check the stereochemical quality of protein structures. J Appl Crystallogr 26:283–291

Meyer TE (1985) Isolation and characterization of soluble cytochromes, ferredoxins and other chromophoric proteins from the halophilic phototrophic bacterium *Ectothiorhodospira halophila*. Biochim Biophys Acta 806:175–183

Meyer TE, Yakali E, Cusanovich MA, Tollin G (1987) Properties of a water-soluble, yellow protein isolated from a halophilic phototrophic bacterium that has photochemical activity analogous to sensory rhodopsin. Biochemistry 26:418–423

Meyer TE, Tollin G, Hazzard JH, Cusanovich MA (1989) Photoactive yellow protein from the purple phototrophic bacterium, *Ectothiorhodospira halophila*: quantum yield of photobleaching and effects of temperature, alcohols, glycerol, and sucrose on kinetics of photobleaching and recovery. Biophys J 56:559–564

Pellequer J-L, Wager-Smith KA, Kay SA, Getzoff ED (1998) Photoactive yellow protein: a structural prototype for the three-dimensional fold of the PAS domain superfamily. Proc Natl Acad Sci USA 95:5884–5890

Perman B, Srajer V, Ren Z, Teng T, Pradervand C, Ursby T, Bourgeois D, Schotte F, Wulff M, Kort R, Hellingwerf K, Moffat K (1998) Energy transduction on the nanosecond time scale: early structural events in a xanthopsin photocycle. Science 279:1946–1950

Ren Z, Perman B, Srajer V, Teng TY, Pradervand C, Bourgeois D, Schotte F, Ursby T, Kort R, Wulff M, Moffat K (2001) A molecular movie at 1.8 angstrom resolution displays the photocycle of photoactive yellow protein, a eubacterial blue-light receptor, from nanoseconds to seconds. Biochemistry 5:13788–13801

Rubinstenn G, Vuister GW, Mulder FAA, Düx PE, Boelens R, Hellingwerf KJ, Kaptein R (1998) Structural and dynamic changes of photoactive yellow protein during its photocycle in solution. Nat Struct Biol 5:568–570

Ryckaert JP, Ciccotti G, Berendsen HJC (1977) Numerical integration of cartesian equations of motion of a system with constraints: molecular dynamics of n-alkanes. J Comput Phys 23:327–341

Scott WRP, Hünenberger PH, Tironi IG, Mark AE, Billeter SR, Fennen J, Torda AE, Huber T, Krüger P, van Gunsteren WF (1999) The GROMOS biomolecular simulation program package. J Phys Chem A 103:3596–3607

Shiozawa M, Yoda M, Kamiya N, Asakawa N, Higo J, Inoue Y, Sakurai M (2001) Evidence for large structural fluctuations of the photobleached intermediate of photoactive yellow protein in solution. J Am Chem Soc 123:7445–7446

Smith PE, van Gunsteren WF (1994) Consistent dielectric properties of the simple point charge and extended simple point charge water models at 277 and 300 K. J Chem Phys 100:3169–3174

Sprenger WW, Hoff WD, Armitage JP, Hellingwerf KJ (1993) The eubacterium *Ectothiorhodospira halophila* is negatively phototactic, with a wavelength dependence that fits the absorption spectrum of the photoactive yellow protein. J Bacteriol 175:3096–3104

Tironi IG, Sperb R, Smith PE, van Gunsteren WF (1995) A generalized reaction field method for molecular dynamics simulations. J Chem Phys 102:5451–5459

Ujj L, Devanathan S, Meyer TE, Cusanovich MA, Tollin G, Atkinson GH (1998) New photocycle intermediates in the photoactive yellow protein from *Ectothiorhodospira halophila*: picosecond transient absorption spectroscopy. Biophys J 75:406–412

van Aalten DMF, Hoff WD, Findlay JBC, Crielaand W, Hellingwerf KJ (1998) Concerted motions in the photoactive yellow protein. Protein Eng 11:873–879

van Aalten DMF, Crielaard W, Hellingwerf KJ, Joshua-Tor L (2000) Conformational substates in different crystal forms of the photoactive yellow protein: correlation with theoretical and experimental flexibility. Protein Sci 9:64–72

Van Beeumen JJ, Devreese BV, Van Bun SM, Hoff WD, Hellingwerf KJ, Meyer TE, McRee DE, Cusanovich MA (1993) Primary structure of a photoactive yellow protein from the phototrophic bacterium *Ectothiorhodospira halophila*, with evidence for the mass and the binding site of the chromophore. Protein Sci 2:1114–1125

van Gunsteren WF, Billeter SR, Eising AA, Hünenberger PH, Krüger P, Mark AE, Scott WRP, Tironi IG (1996) Biomolecular simulation: the GROMOS96 manual and user guide, Vdf Hochschulverlag an der ETH Zürich, Zürich, Switzerland

Xie A, Hoff WD, Kroon AR, Hellingwerf KJ (1996) Glu46 donates a proton to the 4-hydroxycinnamate anion chromophore during the photocycle of photoactive yellow protein. Biochemistry 35:14671–14678

Xie A, Kelemen L, Hendriks J, White BJ, Hellingwerf KJ, Hoff W (2001) Formation of a new buried charge drives a large-amplitude protein quake in photoreceptor activation. Biochemistry 40:1510–1517

Yamato T, Niimura N, Go N (1998) Molecular dynamics study of femtosecond events in photoactive yellow protein after photoexcitation of the chromophore. Proteins 32:268–275